# ENHANCED CLIMATIC WARMING IN THE TIBETAN PLATEAU DUE TO DOUBLE CO2: A MODEL STUDY

*Baode Chen*
*University of Maryland Baltimore County, Baltimore, MD 21250*

*Winston C. Chao*
*NASA/Goddard Space Flight Center, Greenbelt, MD USA*

*Xiaodong Liu*
*Institute of Earth Environment, Chinese Academy of Sciences, Xian, China*

To be submitted to ***Climate Dynamics***

Popular Summary

The NCAR Regional Climate Model version 2 (RegCM2) is used to investigate the enhanced climatic warming in the Tibetan Plateau (TP) due to double $CO_2$. With the RegCM2 driven by time-dependent lateral fields from output of the NCAR Climate System Model (CSM), two experiments, a 1-year present-day run and 1-year doubled $CO_2$ run, have been conducted. A remarkable elevation-dependency is found in the simulated ground temperature change, i.e. more pronounced warming at high elevation than low elevation, especially so in the winter and spring seasons. This result is consistent with the observational study. From analysis of surface energy budget, the elevation dependency of enhanced ground warming is caused by the snow-albedo feedback resulted from snow cover depletion in higher elevation as well as the enhanced precipitation in lower elevations.

# Enhanced Climatic Warming in the Tibetan Plateau Due to Double $CO_2$: A Model Study

Baode Chen[1,*], Winston C. Chao[2] and Xiaodong Liu[3]

[1]GEST Center, University of Maryland, Baltimore County, Baltimore, MD, USA

[2]NASA/Goddard Space Fight Center, Greenbelt, MD, USA

[3]Institute of Earth Environment, Chinese Academy of Sciences, Xian, China

October 2001

* *Corresponding author address:* Dr. Baode Chen, GSFC/NASA, Mail Code 913, Greenbelt, MD20711, USA. E-mail: bdchen@climate.gsfc.nasa.gov

## Abstract

The NCAR regional climate model (RegCM2) with time-dependent lateral meteorological fields provided by a 130-year transient increasing $CO_2$ simulation of the NCAR Climate System Model (CSM) has been used to investigate the mechanism of enhanced ground temperature warming over the TP. From our model results, a remarkable tendency of warming increasing with elevation is found for the winter season, and elevation dependency of warming is not clearly recognized in the summer season. This simulated feature of elevation dependency of ground temperature is consistent with observations. Based on an analysis of surface energy budget, the short wave solar radiation absorbed at the surface plus downward long wave flux reaching the surface shows a strong elevation dependency, and is mostly responsible for enhanced surface warming over the TP. At lower elevations, the precipitation forced by topography is enhanced due to an increase in water vapor supply resulted from a warming in the atmosphere induced by doubling $CO_2$. This precipitation enhancement must be associated with an increase in clouds, which results in a decline in solar flux reaching surface. At higher elevations, large snow depletion is detected in the $2xCO_2$ run. It leads to a decrease in albedo, therefore more solar flux is absorbed at the surface. On the other hand, much more uniform increase in downward long wave flux reaching the surface is found. The combination of these effects (i.e. decrease in solar flux at lower elevations, increase in solar flux at higher elevation and more uniform increase in downward long wave flux) results in elevation dependency of enhanced ground temperature warming over the TP.

## 1. Introduction

There are growing concerns over climate change in high elevation areas. Specifically, the climatic warming induced by greenhouse gases could severely impact on human activities and ecosystems in these regions. A number of studies have presented evidences that surface climate change associated with global warming at high elevation sites shows more pronounced warming than at low elevations, i.e. an elevation dependency of climatic warming. Beniston *et al.* (1997) indicated that, as far as the same latitudes of northern land are concerned, the observed surface temperatures change seems to be related to elevation. In addition, Beniston and Rebetez (1996) found that surface climate change in the Swiss Alps in association with global warming displayed an altitudinal dependency. In the Tien Shan of central Asia, during the last half of the 20th century, the warming trend in regions over 2000 m above sea level (a.s.l.) appeared to be greater than that below 2000 a.s.l. (e.g. Aizen *et al.*, 1997). By using an early version of the National Center of Atmosphere Research (NCAR) regional climate model, Giorgi *et al.* (1997) show that snow-albedo feedback may be responsible for the excessive warming in the Swiss Alps. From an ensemble of climate change experiments with increasing greenhouse gases and aerosols using an air-sea coupled climate model, Fyfe and Flato (1999) found a marked elevation dependency of the simulated surface screen temperature increase over the Rocky Mountains.

The Tibetan Plateau (TP) is located in central Asia with a mean elevation of more than 4000 m a.s.l. and an area of about 2.3 x $10^6$ $km^2$. It is surrounded by the Earth's

highest mountains, such as the Himalayas, Pamir, Kunlun Shan and others and exerts profound thermal and dynamical influences on the local weather and climate as well as on atmospheric circulation in the Northern Hemisphere (e.g. Manabe and Terpstra, 1974; Yeh and Gao, 1979; Manabe and Broccoli, 1990; Yanai *et al.*, 1992; Kutzbach *et al.*, 1993). The analysis of ice core on the TP indicates significant increase of surface temperature over the last few decades (e.g. Thompson *et al.*, 1993; Yao *et al.*, 1995), which appears to be associated with a retreat of most mountain glaciers on the TP (see Tang *et al.*, 1998 for details). Using almost all the available instrumental records, Liu and Chen (2000) showed that the main portion of the TP has experienced significant warming since the mid-1950s, especially in winter, and linear rates of ground temperature increase over the TP during the period of 1955-1996 are about 0.16°C/decade for the annual mean and 0.32°C/decade for the winter mean which exceed those for the same latitudinal zone in the Northern Hemisphere in the same period. In addition, they found that there is a tendency for the warming trend to increase with elevation in the TP as well as its surrounding areas.

With its vast area the TP has unique topography, landscape and climate compared with other high elevation regions. It is natural to consider that the climate warming and its elevation dependency over the TP are closely associated with its inherent complexity of topography and climate variability among various terrestrial regimes. Therefore, in order to investigate a topographically enhanced climate warming over the TP, using high-resolution models is essential. In this paper, we will investigate the mechanism of elevation dependency of climatic warming in the TP by using a high resolution regional

climate model.

In the next section the model used and experiments design will be outlined. Section 3 shows the enhanced climatic warming simulated from two one-year integrations driven by the lateral boundary forcing from the National Center for Atmospheric Research (NCAR) Climate System Model (CSM) run. Section 4 will discuss the surface energy budget and hydrologic regime. Conclusion and discussion will be presented in Section 5.

## 2. Description of model used and experiment design

The latest version of the NCAR regional climate model version 2 (RegCM2) is used. The dynamical component of the RegCM2 is essentially the same as that of the MM4 (The NCAR-Pennsylvania State University Meso-scale Model version 4), which is a compressible, grid point model with hydrostatic balance and vertical $\sigma$-coordinates. Exceptions are the use of a split-explicit time integration scheme and of an algorithm for reducing horizontal diffusion in the presence of steep topographical gradients (Giorgi et al. 1993a,b). A number of physics parameterization schemes have been adopted by the model's developers for applications to climate studies. The radiative transfer package is from that of the NCAR Community Climate Model version 3 (CCM3), and the boundary layer scheme from Holtslag et al. (1990). The latest version of BATS 1E (Biosphere-Atmosphere Transfer Scheme) (Dickinson et al. 1992) was incorporated into the model to perform the surface physics calculations. The mass flux scheme of Grell (1993) was implemented for cumulus convection parameterization.

An area covering the entire TP was selected for our purpose. Fig. 1 shows the model topography for the selected domain. A 60 km grid size and 14 levels with the model top at 80 hPa are used. The climate of the selected region where a large variety of land surface types, from tropical rain forest to desert, exist, is characterized by remarkable monsoon circulations, and the spatial pattern of precipitation is frequently enhanced by topographical forcing. To evaluate the model's performance in this area, the RegCM2 was first integrated for a 4-month period (June - September, 1994) by using the TOGA analyses of Europe Center of Medium Range Weather Forecasting (ECMWF) as the lateral boundary forcing. The results (not shown) indicate that the model did fairly well in the simulations of precipitation, surface temperature and monsoon circulations. Furthermore, Kato et al (2001) evaluated the performance of RegCM2 for the simulation of climate change in East Asia caused by global warming, and indicated that the typical precipitation phenomenon during the winter and summer monsoon is well reproduced in the RegCM.

Two 1-year runs have been carried out with time-dependent lateral meteorological fields provided by a 130-year transient increasing $CO_2$ simulation of the NCAR CSM. From the 130-year simulation, one year is selected as the control run when $CO_2$ level being held at the present day value (355 ppm) and another as the $2XCO_2$ run when doubling $CO_2$ being achieved

**3. The enhanced climatic warming signal detected from the experiments.**

*a. An overview of the CSM forcing.*

The lateral forcing used for our experiments is from a 130-year transient increasing $CO_2$ run produced by the NCAR CSM, in which atmospheric $CO_2$ is increased at a rate of 1% $yr^{-1}$. Meehl et al.(2000) indicated that the simulated globally averaged surface air temperature increase near the time of $CO_2$ doubling is about 1.43°C, with an increase of globally averaged precipitation of 2%. In addition, the greatest warming is found in the winter hemisphere at high latitudes, particularly in the Northern Hemisphere during December-February (DJF). As compared with other global coupled models, global warming due to increased $CO_2$ is relatively low in the NCAR CSM (Kattenberg et al. 1996).

*b. Warming in the Tibetan Plateau.*

The ground temperature differences between RegCM2 $2XCO_2$ and control experiments are plotted in Fig. 2 as a function of elevation over the model grid points for summer, winter and annual means. In Fig. 2, topographical elevation is grouped into 10 categories with a 500-m interval, i.e., 0.5 - 1.0 km, 1.0-1.5 km,...,5.0-5.5 km, and the value of temperature difference is obtained by averaging results over all grid points in each elevation category. Table 1 is the number of grid points used in the averaging for each elevation category. It varies from a maximum of 895 for 0.5-1.0 km category to a minimum of 69 for elevation between 3.5-4.0 km. Notice that there are 128 points for the highest elevation from 5.0-5.5 km.

The annually averaged ground temperature warming is from 0.9° C at the lowest elevation to 2.6°C at the highest sites. Considering that the CSM shows a relatively weak sensitivity to $CO_2$ concentration and that a relatively large sample size to produce average, the simulated warming is quite profound in the TP.

A remarkable tendency of ground temperature warming increasing with elevation can be found for the winter season (November to February). The maximum temperature increase is 3.7°C at 4.5 to 5.5 km elevation, and the warming is 3.1°C more than that at 0.5 to 1.0 km. For summer (June to September) the elevation dependency is not clearly recognized. It can be seen that there is a maximum of 2.2°C warming at 2.5-3.0 km and weaker warming below or above. This result is consistent with Liu and Chen's observational study (2001).

Fig. 3 shows the winter ground temperatures as simulated from the control run (Fig. 3a), the $2XCO_2$ run (Fig. 3b) and the difference between them (Fig. 3c). The ground temperature patterns closely follow the topographic characteristics of the TP with cooler temperature at the higher altitudes and strong temperature gradient corresponding to large elevation gradient. In comparison with the simulation from the CSM (not shown), the ground temperature produced by the RegCM2 shows more detailed structure and the feature of topographic dependency is much more evident. In Fig. 3c, it can be seen that the ground temperature warming almost covers the entire TP with two maximum bands along the southeastern and western slopes. In addition, a cooling area is located in the northern side of the TP.

## 4. Surface processes responsible for the elevation dependency in the TP

*a. Surface energy budget*

The ground temperature is determined by surface energy exchanges. Among various kinds of energy received and emitted by the surface, from the viewpoint of physical processes, are the absorbed solar flux plus the downward longwave flux at the surface ($S_g + F_{IR}^{\downarrow}$), infrared radiation flux emitted from the surface ($\sigma T_g^4$), surface sensible heating flux and latent heating flux. In order to demonstrate the roles of surface energy exchanges associated with the surface condition changes in the local temperature response, an analysis of the surface energy balance will be made.

The differences between the $2XCO_2$ and control run in ($S_g + F_{IR}^{\downarrow}$), long wave surface emission, surface sensible heat flux and latent heat flux are shown in Figure 4 as a function of elevation for the winter season. It can be seen that the $2XCO_2$ run ($S_g + F_{IR}^{\downarrow}$) is greater than the control run at all elevations. The difference becomes enlarged with the elevation increase showing a strong elevation dependency, which is mostly responsible for the enhanced surface warming at higher elevations. The increase in $2XCO_2$ run ($S_g + F_{IR}^{\downarrow}$) is mainly offset by increased surface emission of infrared radiation as a result of the greater ground temperature. There is little elevation signal found in the surface latent heat flux, and fluctuation is evident in the sensible heat.

Figure 5 illustrates the differences between $2\times CO_2$ and control run in surface absorbed

solar flux ($S_g$) as well as downward longwave flux ($F_{IR}^{\downarrow}$) as functions of elevations. The surface absorbed solar radiation shows a decline for the $2\times CO_2$ run in an elevation range of 5 km to 25 km and the decrease becomes weaker as elevation increasing. As the topography reaches up to more than 25 km altitude the $S_g$ difference turns into positive values indicating an enhancement in solar radiation absorbed at the surface for the $2\times CO_2$ run. Although a negative value displays at elevation of 45-50 km, by and large an elevation dependency is quite evident in $S_g$. On the other hand, the downward longwave radiative flux at the surface increases at all elevations for the $2\times CO_2$ run, and the increase appears to be a little stronger at higher elevations, in particular, in the range of 30 km to 50 km. However, on the whole, $F_{IR}^{\downarrow}$ increase at each individual elevation category is rather uniform for the $2\times CO_2$ run. It is conceivable that the enhancement in $F_{IR}^{\downarrow}$ for the $2\times CO_2$ run is mostly due to the intensified "greenhouse effect" as a result of doubling $CO_2$ in the CSM boundary forcing and in the local radiative transfer calculation of the RegCM2 as well.

In summary, the less solar flux absorbed at the surface in lower elevations and more solar flux absorbed in higher elevations combined with more uniform enhancement in the downward long wave flux produce an elevation dependency in the ($S_g + F_{IR}^{\downarrow}$), which results in elevation dependency of enhanced ground temperature warming over the TP.

*b. Hydrological regime and the solar flux absorbed at the surface.*

The elevation dependency of enhanced ground temperature warming around the TP is a direct result from an elevation dependency of the solar flux absorbed at the surface. As pointed out by Giorgi et al (1997), the snow-albedo feedback and changes in precipitation regime can provide strong elevation-dependent forcing or modulation for the surface climate change signal through affecting $S_g$.

The precipitation from the control run and $2\times CO_2$ run along with the difference between them are plotted as functions of elevations in Fig. 6 for the winter season. It is found that the $2\times CO_2$ run precipitation is enhanced at elevations below 4 km with relatively larger enhancement at lower elevations. The precipitation at very high elevations (>4 km) decreases very dramatically for both runs and the difference between two runs becomes very small. This result may be expected because of the lack of available water vapor at very high locations during the winter season. Moreover, in the cold season, the most important contribution to precipitation processes around the TP is topographic forcing which is, however, is largely associated with the gradient of topography rather than topography itself. Figs 7a-c show the winter season mean precipitation simulated by both control and $2\times CO_2$ runs (Fig. 7a and 7b) together with the $2\times CO_2$-minus-control precipitation difference (Fig. 7c). The precipitation produced by both runs is mainly concentrated along the southwestern side of the TP where the greatest topography gradient is in close vicinity to and the water vapor supply is abundant, suggesting strong topographic forcing. From the difference of $2\times CO_2$-minus-control precipitation (Fig. 7c), the larger enhancement of rainfall occurs at the southwestern side of the mountains in the doubling $2\times CO_2$ run. The enhanced precipitation around these regions where elevations

are below 3.5 km, suggests an increase in clouds which will result in a relatively larger decrease in solar flux reaching the surface as shown in Fig 5.

Fig. 8 depicts snow depth as a function of elevations for the control and $2xCO_2$ runs along with the difference of $2xCO_2$-minus-control. As shown in Fig. 8, the largest snow accumulation occurs at elevations of 35 km to 40 km in the control run, and is dramatically reduced in the $2xCO_2$ run. This large snow depletion leads to a decrease in surface albedo, as a result, more solar flux is absorbed at the surface.

## 5. Summary and discussion

The NCAR RegCM2 with time-dependent lateral meteorological fields provided by a 130-year transient increasing $CO_2$ simulation of the NCAR CSM has been used to investigate the mechanism of enhanced ground temperature warming over the TP. From our model results, a remarkable tendency of warming increasing with elevation is found for the winter season, and elevation dependency of warming is not clearly recognized in the summer season. The simulated feature of elevation dependency of ground temperature is consistent with observations. Based on an analysis of surface energy budget, the short wave solar radiation absorbed at the surface plus downward long wave flux reaching the surface shows a strong elevation dependency, and is mostly responsible for enhanced surface warming over the TP. At lower elevations, the precipitation forced by topography is enhanced due to an increase in water vapor supply resulted from a warming in the atmosphere induced by doubling $CO_2$. This precipitation enhancement must be associated

with an increase in clouds, which will result in a decline in solar flux reaching the surface. At higher elevations, large snow depletion is detected in the $2xCO_2$ run, as a result of snow depletion, which leads to a decrease in albedo, more solar flux is absorbed at the surface. On the other hand, much more uniform increase in downward long wave flux reaching the surface is found. Therefore, the combination of these effects (i.e. decrease in solar flux at lower elevations, increase in solar flux at higher elevation and more uniform increase in downward long wave flux) results in enhanced ground temperature warming over the TP.

Both Giorgi et al (1997) and Fyfe et al (1999) have shown that the snow-albedo feedback mechanism plays a major role in elevation dependency of the surface climate change signal in the Alps and Rocky mountains based on the results from two models with quite different resolutions. In particular, the model used by Fyfe et al (1999) has a relatively coarse T32 resolution, but as they claimed, the topography of the Rockies in the model reaches high enough over a large enough area to be able to support appreciable winter and spring snow cover. In both study, reduced snow cover in high elevation is essential to the elevation effect. Compared with the Alps and Rocky mountain complexes, the TP has much larger area and higher elevations as well as far more various terrestrial regimes. From the NCAR CSM transient increasing $CO_2$ run (having a T42 resolution) used as the lateral forcing for the RegCM2 in our study, there is no clear elevation dependency detected over the TP (not shown) although snow depletion occurs when the $CO_2$ reaches doubling level, suggesting other factors may play a role in the topography dependency in the TP. Our model results from the RegCM2 indicate that the enhanced

precipitation in the southwestern slope of the TP, where the maximum topography gradient and windward side are located at, is responsible for changes in the solar radiation absorbed at the surface at lower elevations. This topography forcing precipitation is certainly underestimated in the NCAR CSM because of a much smoother topographical representation for the TP. We also speculate that the precipitation induced by topography has little influence on the elevation dependency in the Alps and Rocky mountains because they have much smaller areas and topography gradients.

During the summer season, the climate over the TP is essentially characterized by summer monsoon circulation, especially in the south of the plateau. In addition to precipitation induced by low level convergence associated with the monsoon flows and upward motions dynamically forced by topography, at high elevations surface heating will also destabilize the overlying atmosphere and enhance convective precipitation. Thus the local response to global warming over the TP is much more complicated than that in winter. In order to get more reliable results, accurate simulation of summer monsoon is essential for either GCM or regional model.

Finally, it should be pointed out that our results reported in this paper should not be viewed as a quantitative estimation of climate change or climate predication because they are only based on sensitivity of climate to atmospheric $CO_2$ concentration. Our purpose is only to suggest a physical interpretation to elevation effect of climatic warming which has an observational counterpart. Much more numerical experiments need to be done in order to get quantified results.

*Acknowledgments:* The authors would like to thank Drs. J. Qian and X. Bi for providing the model code and data. This work is supported by NASA/Office of Earth Science. XD Liu also thanks for support from Chinese Academy of Sciences

## References


Aizen, V. B., M. Aizen, J. M. Melack and J. Dozier, 1997: Climatic and hydrologic changes in the Tien Shan, central Asia, *J. Climate*, **10**, 1393-1404.

Beniston, M. and M. Rebetez, 1996: Regional behavior of minimum temperatures in Switzerland for the period 1979-1993. *Theor. Appl. Climatol.*, **53**, 231-244.

Beniston, M., H. F. Diaz and R. S. Bradley, 1997: Climatic change at high elevation sites: An overview, *Climatic Change*, **36**, 233-251.

Dickinson, R. E., and A. Henderson-Sellers, and P. J. Kennedy, 1993: Biosphere-Atmosphere Transfer Scheme (BATS) Version 1e as Coupled to the NCAR Community Climate Model. NCAR Tech. Note NCAR/TN-387+STR, 72pp

Fyfe, J. C, and G. M. Flato, 1999: Enhanced climate change and its detection over the Rocky Mountains, *J. Climate,* **12,** 230-243.

Giorgi, F., J. Hurrell, M. R. Marinucci and M. Beniston, 1997: Elevation dependency of the surface climate change signal: A model study, *J. Climate,* **10**, 288-296.

Giorgi, F., M. R. Marinucci, and G. T. Bates, 1993a: Development of a second generation regional climate (RegCM2): Boundary layer and radiative transfer processes. *Mon. Wea. Rew.* **121,** 2794-2813.

Giorgi, F., M. R. Marinucci, G. De Canio, and G. T. Bates, 1993b: Development of a second generation regional climate (RegCM2): Convective processes and assimilation of lateral boundary conditions. *Mon. Wea. Rew.* **121,** 2814-2832

Grell, G. A., J. Dudhia, and D. R. Stauffer, 1994: A description of the fifth generation Penn State/NCAR Mesoscale Model (MM5). NCAR Tech. Note NCAR/TN-398+STR, 121pp

Holtslag, A.A.M., E.I.E. de Bruijn, and H. L. Pan, 1990, A high resolution air mass transformation model for short-range weather forecasting. *Mon. Wea. Rev.* **118**, 1561-1575

Kato, H, K. Nishizawa, H. Hirakuchi, S. Kadokura, N. Oshima, and F. Giorgi, 2001: Performance of RegCM2.5/NCAR-CSM nested system for the simulation of climate change in East Asia caused by global warming, *J. Meteor. Soc. Japan*, **79,** 99-121.

Kattenberg, A., and Coauthors, 1996: Climate models – projections of future climate. *Climate Change 1995: The Science of Climate Change: Contribution of Working Group I to the Second Assessment Report of the Intergovernment Panel on Climatic Change.* J. H. Houghtong et al., Eds., Cambridge University Press, 285-357.

Kutzbach, J. E., W. L. Prell and W. F. Ruddiman, 1993: Sensitivity of Eurasian climate to surface uplift of the Tibetan Plateau, *J. Geology,* **101**, 177-190.

Manabe, S. and T. B. Terpstra, 1974: The Effects of mountains on the general circulation of the atmosphere as identified by numerical experiments, *J. Atmos. Sci.*, **31**, 3-42.

Manabe, S. and A. J. Broccoli, 1990: Mountains and arid climate of middle latitudes, *Science*, **247**, 192-195.

Meehl, G. A. , W. M. Washington, J. M. Arblaster, T. W. Bettge, and W. G. Strand, 2000: Anthropogenic forcing and decadal climate variability in sensitivity experiments of twentieth- and twenty-first-century climate, *J. Climate*, **13,** 3278-3744

Tang, M.-C., G.-D. Cheng and Z.-Y. Lin (eds.), 1998: Contemporary Climatic Variations over the Qinghai-Xizang (Tibet) Plateau and Their Influences on Environments, *Guangdong Science and Technology Press*, Guangzhou, 229pp (in Chinese).

Thompson, L. G., E. Mosley-Thompson, M. E. Davis, N. Lin, T. Yao, M. Dyurgerov, and J. Dai, 1993: "Recent warming": Ice core evidence from tropical ice cores, with emphasis on central Asia, *Global Planet Change*, **7,** 145-156.

Yao, T., G. Lonnie, L. G. Thompson, et al., 1995: Recent warming as recorded in the Qinghai-Tibet cryosphere, *Annals of Glaciology*, **21**, 196-200

Yanai, M., C. Li and Z. Song, 1992: Seasonal heating of the Tibetan Plateau and its effects on the evolution of the summer monsoon, *J. Meteor. Soc. Japan*, **70,** 319-351.

Yeh, T.-C. and Y.-X. Gao et al., 1979: *The Meteorology of the Qinghai-Xizang (Tibet) Plateau,* Science Press, Beijing, 278pp (in Chinese).

Liu, XD and B. Chen, 2000: Climatic warming in the Tibetan Plateau during recent decades,

*Int. J. Climatology.* **20,** 1729-1742

Figure Captions

Fig. 1: Model domain and topography. Units are 100m and the contour interval is 400m.

Fig. 2: Ground temperature difference between $2\times CO_2$ and control run as a function of elevation.

Fig. 3: Simulated ground temperature for a) the control run, b) the $2\times CO_2$ run and c) the differences of the $2\times CO_2$-minus-control run. Topography is shaded and units are °K.

Fig. 4: Difference between $2\times CO_2$ and control run surface fluxes as a function of elevation for the winter season.

Fig.5: Difference between $2\times CO_2$ and control run absorbed solar flux ($S_g$) and downward long wave flux ($F_{lR}^{\downarrow}$) at the surface as a function of elevation for the winter season.

Fig. 6: Difference between $2\times CO_2$ and control run precipitation as a a functi cn cf elevati

$mm \cdot day^{-1}$.

Fig. 8: Difference between $2\times CO_2$ and control run snow depth as a function of elevation, as well as simulated snow depth for the $2\times CO_2$ and the control runs.

Table 1. The numbers of grid points used in the average for each elevation category.

| Elevation (km) | Number of Grid Points |
|---|---|
| 0.5 – 1.0 | 895 |
| 1.0 – 1.5 | 703 |
| 1.5 – 2.0 | 341 |
| 2.0 – 2.5 | 149 |
| 2.5 – 3.0 | 86 |
| 3.0 – 3.5 | 70 |
| 3.5 – 4.0 | 69 |
| 4.0 – 4.5 | 74 |
| 4.5 – 5.0 | 94 |
| 5.0 – 5.5 | 128 |

Fig. 1

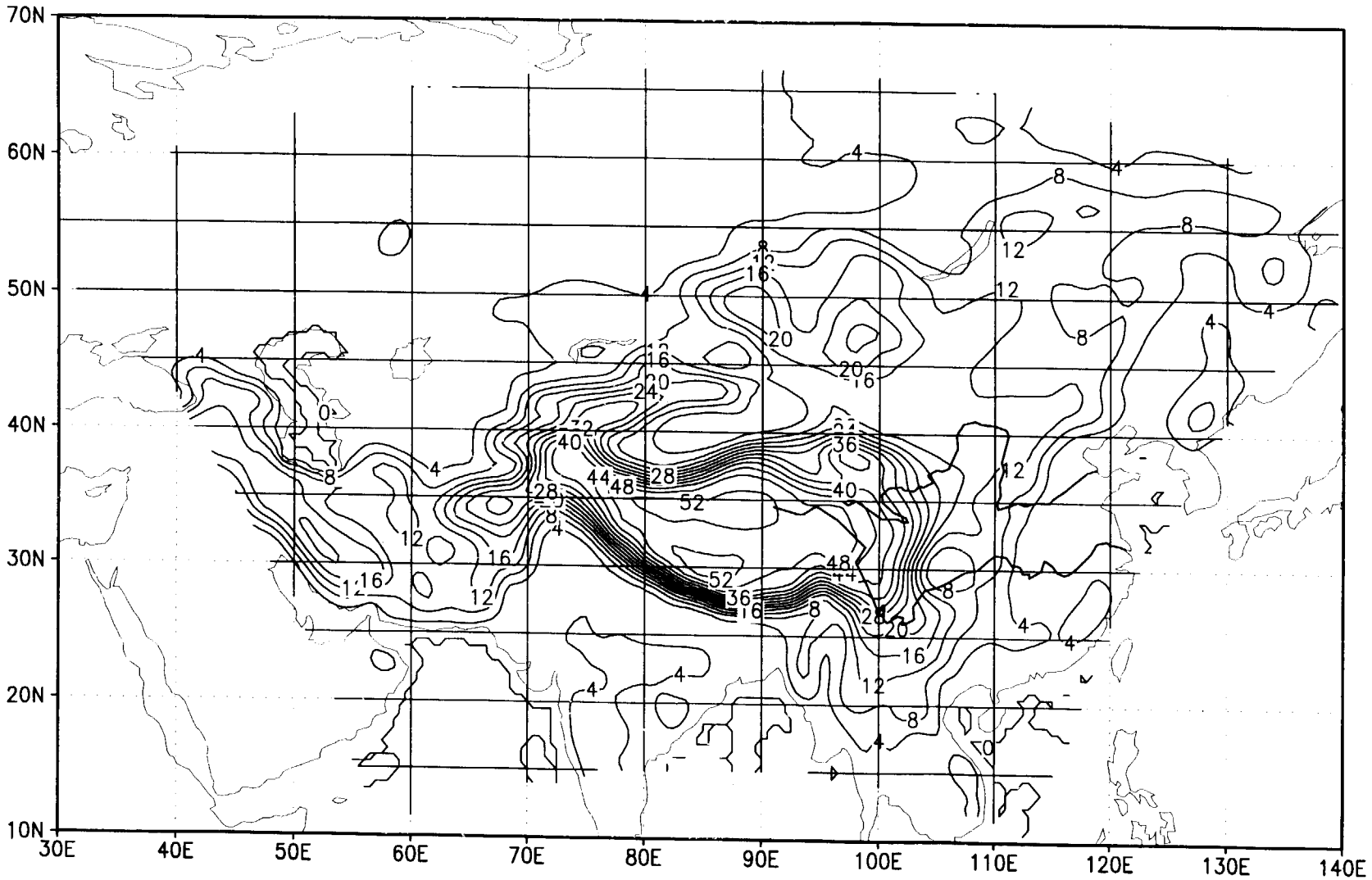
70N
60N
50N
40N
30N
20N
10N
30E
40E
50E
60E
70E
80E
90E
100E
110E
120E
130E
140E

Fig. 2

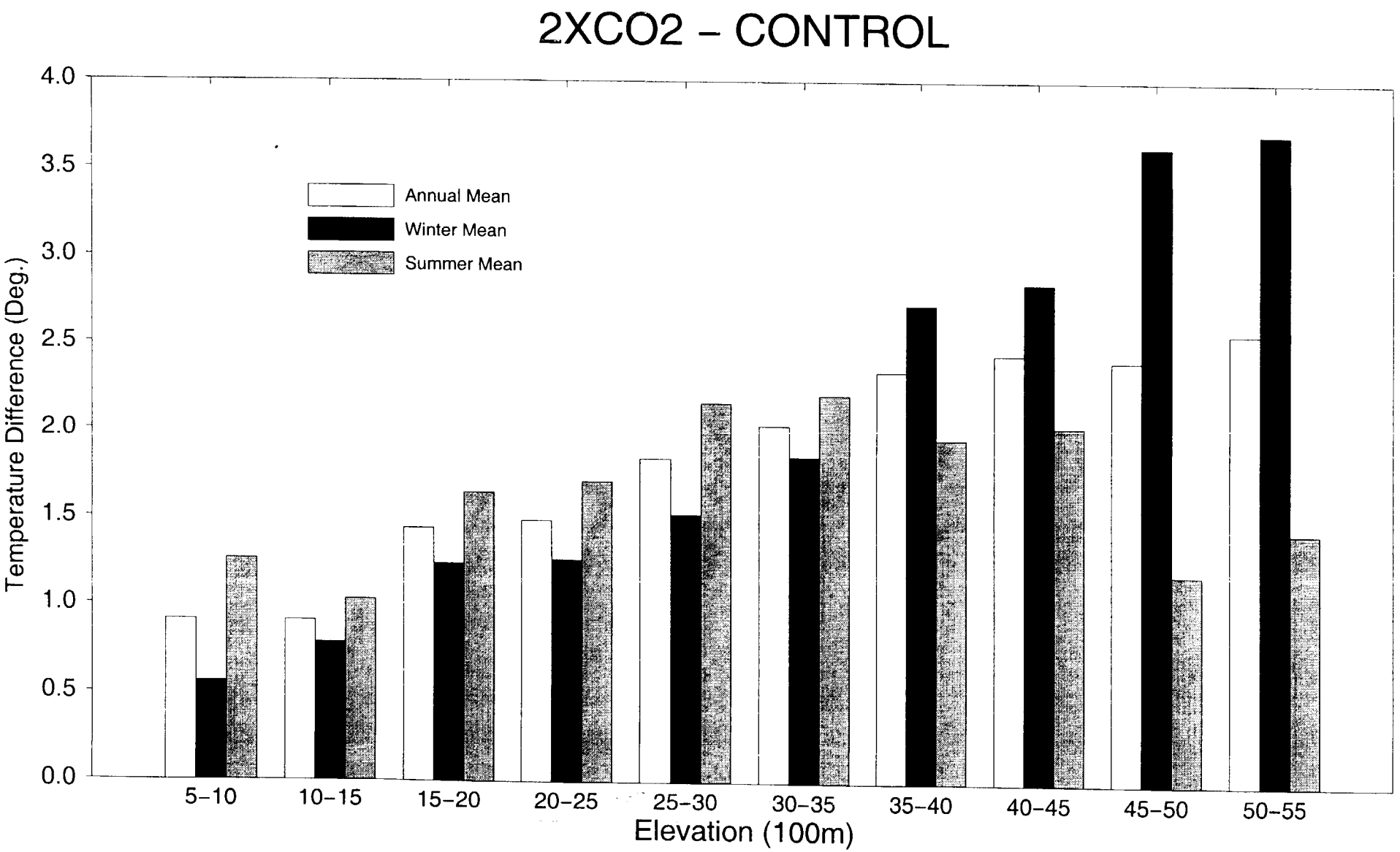
2XCO2 – CONTROL
Annual Mean
Winter Mean
Summer Mean
Temperature Difference (Deg.)
4.0
3.5
3.0
2.5
2.0
1.5
1.0
0.5
0.0
5–10
10–15
15–20
20–25
25–30
30–35
35–40
40–45
45–50
50–55
Elevation (100m)

F 7.3

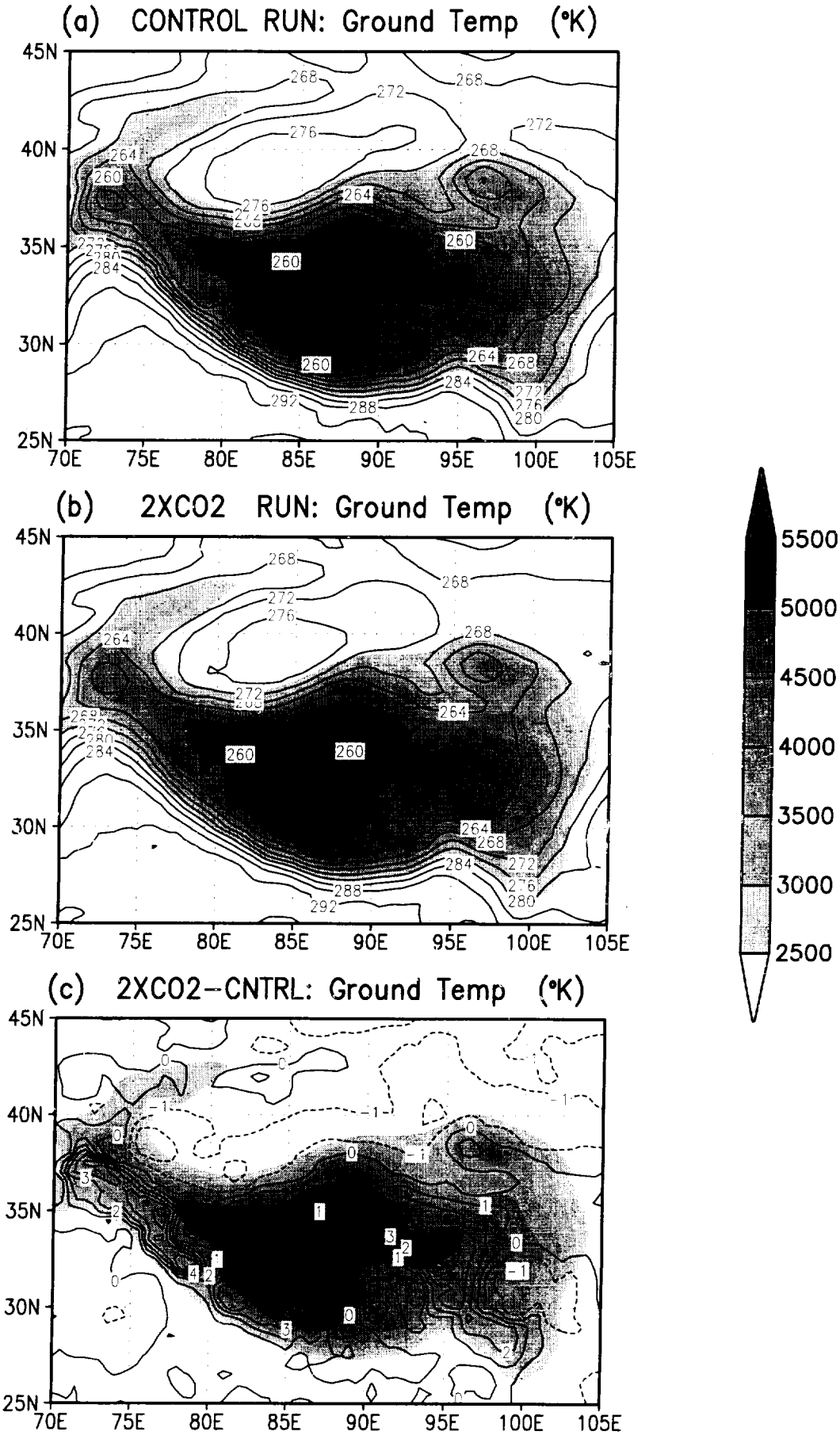
(a) CONTROL RUN: Ground Temp (°K)
(b) 2XCO2 RUN: Ground Temp (°K)
(c) 2XCO2–CNTRL: Ground Temp (°K)
45N
40N
35N
30N
25N
70E
75E
80E
85E
90E
95E
100E
105E
5500
5000
4500
4000
3500
3000
2500

Fig 4

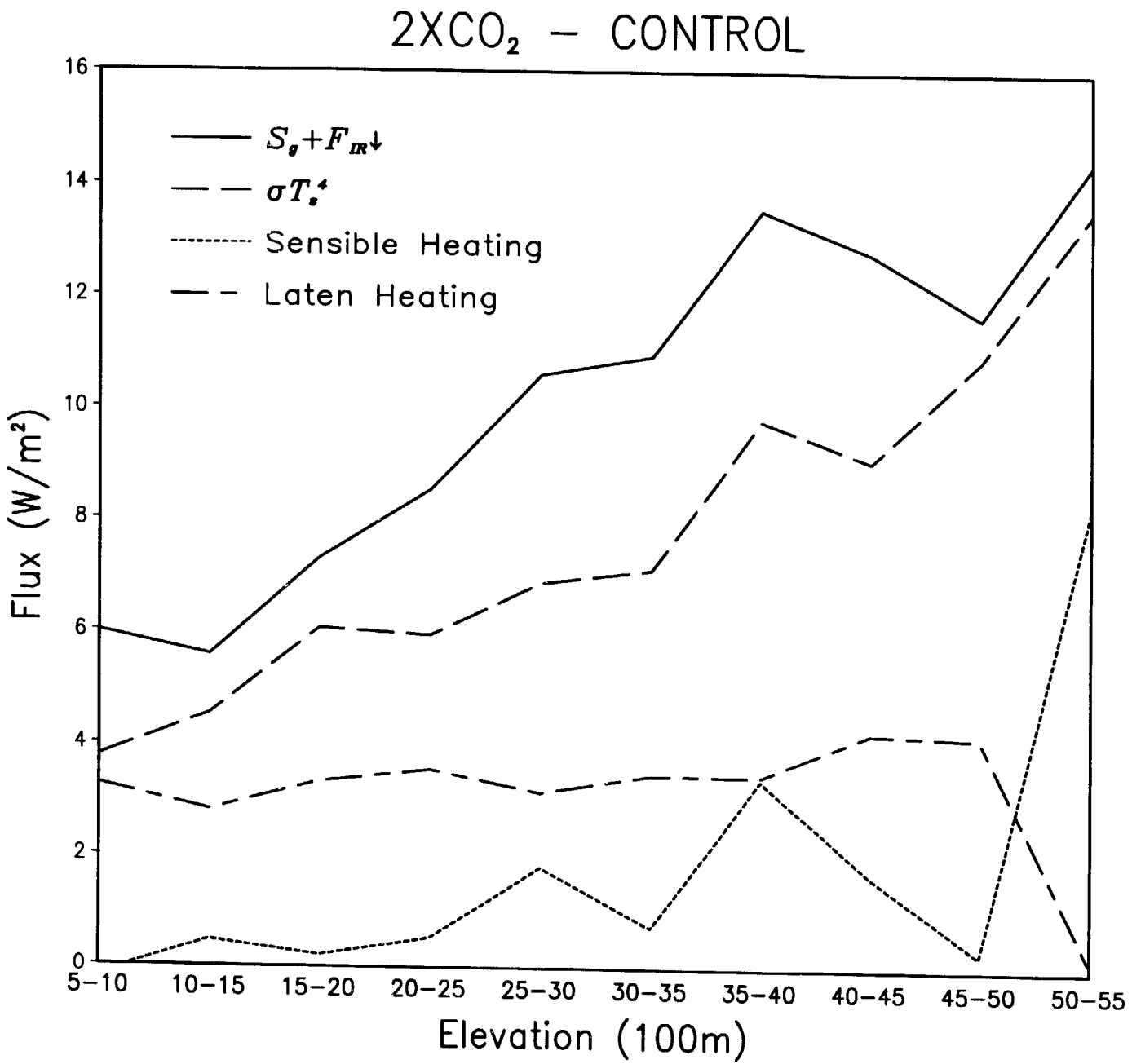
2XCO2 – CONTROL
$S_g+F_{IR}\downarrow$
$\sigma T_s^4$
Sensible Heating
Laten Heating
Flux (W/m²)
0
2
4
6
8
10
12
14
16
5–10
10–15
15–20
20–25
25–30
30–35
35–40
40–45
45–50
50–55
Elevation (100m)

Fig. 5

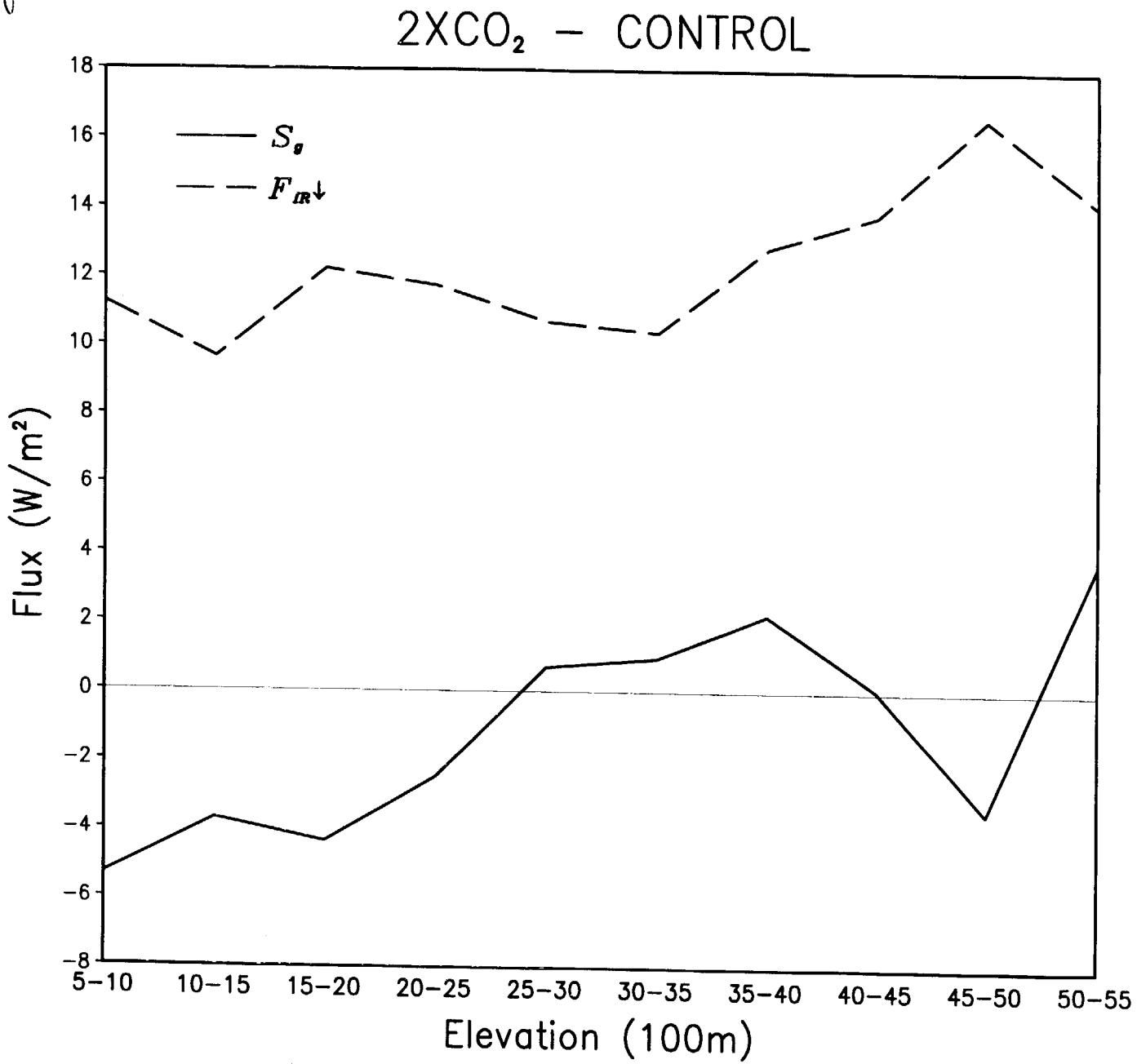
2XCO2 – CONTROL
Sg
FIR↓
Flux (W/m²)
18
16
14
12
10
8
6
4
2
0
−2
−4
−6
−8
5–10
10–15
15–20
20–25
25–30
30–35
35–40
40–45
45–50
50–55
Elevation (100m)

Fig 6

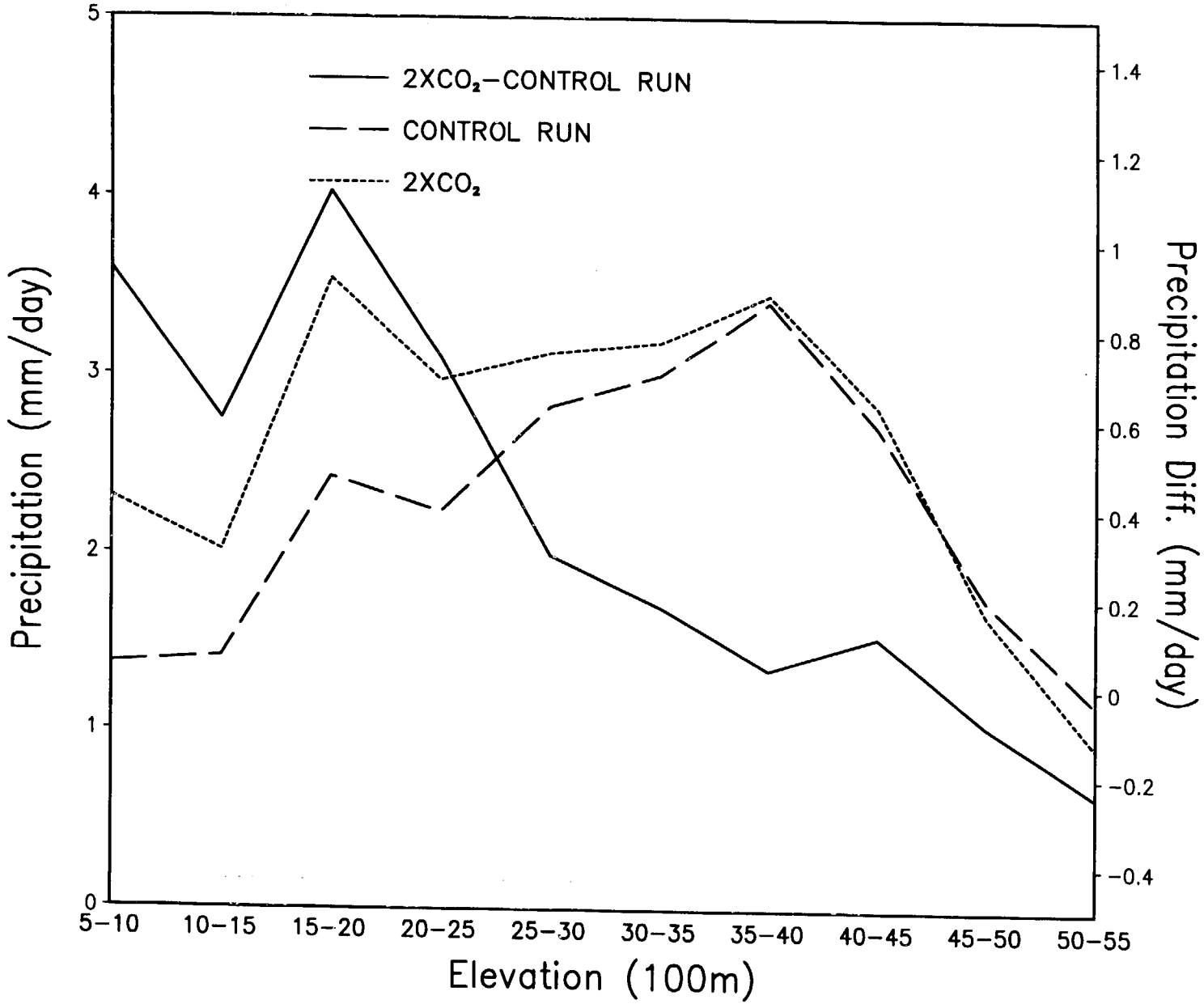
2XCO₂–CONTROL RUN
CONTROL RUN
2XCO₂
Precipitation (mm/day)
Precipitation Diff. (mm/day)
Elevation (100m)
0
1
2
3
4
5
1.4
1.2
1
0.8
0.6
0.4
0.2
0
−0.2
−0.4
5–10
10–15
15–20
20–25
25–30
30–35
35–40
40–45
45–50
50–55

Fig 7

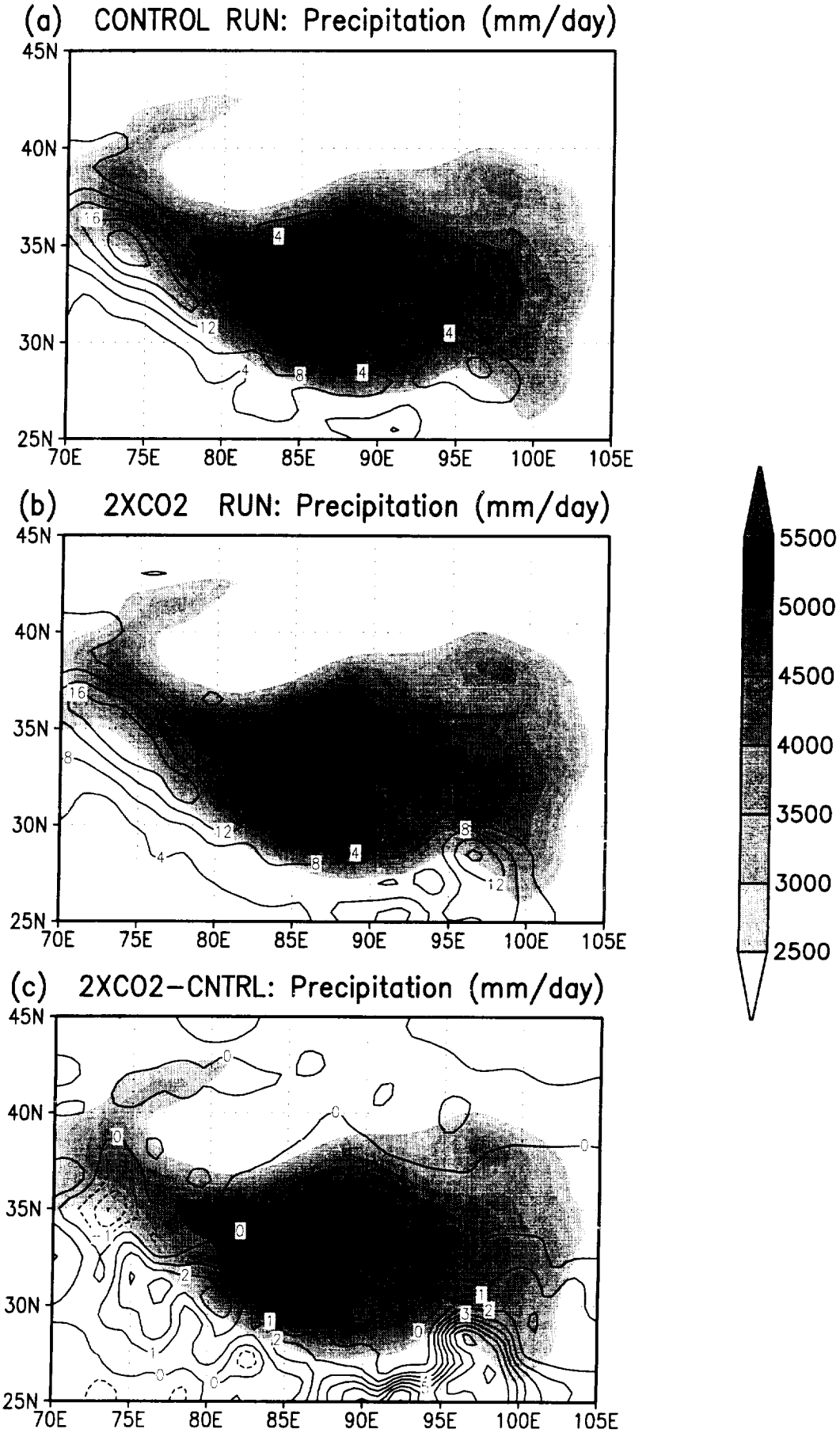
(a) CONTROL RUN: Precipitation (mm/day)
(b) 2XCO2 RUN: Precipitation (mm/day)
(c) 2XCO2−CNTRL: Precipitation (mm/day)
45N
40N
35N
30N
25N
70E
75E
80E
85E
90E
95E
100E
105E
5500
5000
4500
4000
3500
3000
2500

Fig. 8

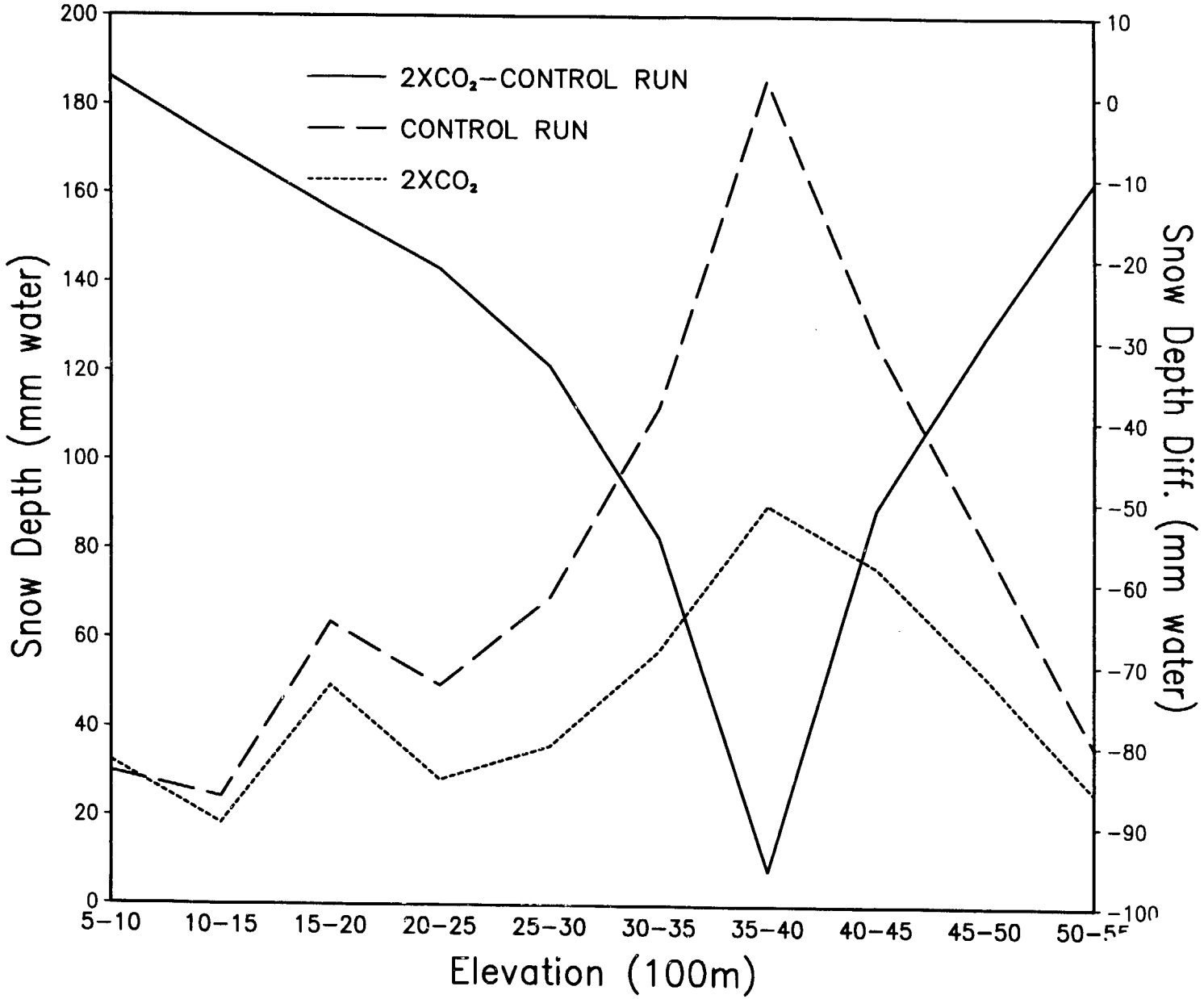
2XCO₂–CONTROL RUN
CONTROL RUN
2XCO₂
Snow Depth (mm water)
Snow Depth Diff. (mm water)
Elevation (100m)
200
180
160
140
120
100
80
60
40
20
0
10
0
−10
−20
−30
−40
−50
−60
−70
−80
−90
−100
5–10
10–15
15–20
20–25
25–30
30–35
35–40
40–45
45–50
50–55